

1A Review of Biochar-Based Catalysts for Chemical Synthesis, 2Biofuel Production, and Pollution Control

3Xinni Xiong¹, Iris K.M. Yu¹, Leichang Cao², Daniel C.W. Tsang*¹, Shicheng Zhang², Yong Sik
4Ok³

5¹ Department of Civil and Environmental Engineering, The Hong Kong Polytechnic University, Hung Hom,
6Kowloon, Hong Kong, China

7² Department of Environmental Science and Engineering, Fudan University, Shanghai 200433, China

8³ Korea Biochar Research Center & School of Natural Resources and Environmental Science, Kangwon National
9University, Chuncheon 24341, Korea

10*Corresponding author: dan.tsang@polyu.edu.hk

11

12Abstract

13This review addresses the use of biochar as a green and versatile catalyst support for emerging
14high-end applications beyond soil remediation, including chemical synthesis and biodiesel
15production from biomass, and pollutant degradation in the environment. Their catalytic
16performances are comparable or even superior to the conventional resin-, silica-, or carbon-based
17catalysts, owing to the favourable intrinsic features of biochar (various functional groups,
18intricate network of structures, etc.). Yet, distinctive active sites are needed for different
19applications. It is highlighted that the active site accessibility for substrates critically determines
20the performance, which is associated with the biochar physicochemical characteristics (-SO₃H
21site density, pore size distribution, surface area, etc.). They show varying significance depending
22on the catalytic sites on biochar, which may be controlled via novel pre-/post-synthesis
23modifications. This review elucidates the links among catalytic performances, physicochemical
24properties, and pyrolysis/modification-induced features, advising the tailored production of
25application-oriented biochar-based catalyst in the future.

26**Keywords:** biochar; solid catalyst; acid-catalyzed conversion; biorefinery; waste valorization.

271. Introduction

28Biochar is a low-cost carbon-rich material derived from a wide variety of waste biomass, such as
29sludge/manure, food waste, and agricultural residues, via pyrolysis with limited oxygen or
30hydrothermal carbonization under high pressure (Tang et al., 2013). The advantageous properties

31including relatively large surface area, high pore volume, long-term stability, and enriched
32surface functional groups have rendered biochar a broad spectrum of potential applications. It has
33played an important role in: (i) soil improvement by increasing the nutrient interactions, soil
34fertility, and crop productivity; (ii) carbon sequestration by suppressing the greenhouse gas
35emissions (Lehmann et al., 2015; Hussain et al., 2017); (iii) soil remediation by immobilizing
36various contaminants through sorption, precipitation, etc. (Ahmad et al., 2014; Rizwan et al.,
372016); as well as (iv) wastewater treatment based on its effective removal of heavy metals,
38organic chemicals, and microbial contaminants from the aqueous system (Mohan et al., 2014; Tan
39et al., 2015; Inyang et al., 2016). Its contaminant removal efficiency can be further improved
40upon engineering modifications such as magnetization, carboxylation, and amination (Rajapaksha
41et al., 2016a). In recent years, the applications of biochar have been extending to the high-end
42fields such as energy and healthcare industry, in view of its economical synthesis, sustainability
43merits, and manoeuvrable characteristics (Ok et al., 2015).

44The conversion of biomass to value-added chemicals is one of the emerging applications of
45biochar (Liu et al., 2015a, Zhang et al., 2017). For instance, hydroxymethylfurfural (HMF) arises
46as one of the attractive products with high market value, which is a versatile platform chemical
47for the synthesis of medicines, solvents, polymer, surfactants, and biofuels (Yu et al., 2017a&b;
48Yu and Tsang, 2017). While acid site-bearing resins/polymers or zeolites are widely investigated
49for HMF synthesis, biochar upon functionalization shows a great potential in serving as a
50sustainable alternative. Therefore, it is highly desirable to expand the existing literature for
51boosting the development of application-oriented biochar-based catalyst in the area of
52biorefinery.

53According to the latest reviews on conventional catalytic systems (i.e., mineral acids, commercial
54catalysts, etc.), the biomass valorization is often impeded by the low reactivity of sugar-involved
55reactions and low selectivity of target products due to the side reactions (Zhang et al., 2016; Chen

56et al., 2017a; Yu and Tsang, 2017). To overcome these challenges, it is necessary to tailor the
57catalyst characteristics such as channel size, Brønsted-to-Lewis acid ratio, and hydrophobicity for
58controlling the reaction kinetics. Hence, there is a need to elucidate the significance and possible
59means to manipulate these properties for biochar catalyst-mediated biomass valorization.

60Recently, biochar-based materials have been studied for the catalysis of refinery processes (e.g.,
61syngas cleaning and syngas conversion), biodiesel production, as well as air pollution control
62(Qian et al., 2015; Cha et al., 2016; Lee et al., 2017a). While the current reviews summarize the
63reported performances of different biochars, information on the roles of their physicochemical
64properties remains scattered and diverse. It has been suggested that the surface functionality, for
65example, the $-SO_3H$ groups as the Brønsted acid sites and dispersed metal nanoparticles, governs
66the catalyst efficiency (Liu et al., 2015b). Other properties such as particle strength,
67hydrophobicity, surface area, porosity, and mineral content also emerge as important factors
68depending on the particular applications (Qian et al., 2015). Such divergent knowledge needs to
69be systematically organized and critically reviewed to offer insights for the advancement on
70biochar-based catalysts. It remains uncertain how and to what extent these parameters determine
71the catalytic performances in wide-ranging reactions. Therefore, in-depth understanding on the
72interrelations between the catalytic activity and physicochemical properties is required for
73synthesizing purpose-driven biochar by novel pre- or post-synthesis methods.

74This review summarizes the innovative applications of biochars as catalysts in: (i) chemical
75synthesis from biomass, (ii) biodiesel production, and (iii) air and water pollution control. For
76each application, the catalytic performances are scrutinized to elucidate the critical
77physicochemical properties via comparison to carbon-based alternatives and conventional solid
78catalysts. Existing and potential methods for biochar synthesis and tailoring to serve different
79catalytic applications are discussed.

802. Tailoring biochar properties for catalytic application

81The physicochemical properties of biochar, including acid density (-SO₃H in particular), surface
82area, pore size and volume, surface oxygen functional groups, and metal dispersion and
83speciation, are conducive to the performance of biochar-based catalysts (will be discussed in
84Section 3-5). Therefore, it is important to control these properties by manoeuvring the protocol of
85catalyst preparation.

862.1 Thermochemical production of biochar

87Biochar is usually produced via pyrolysis of biomass under limited oxygen supply at the
88temperature ranging from 300 to 800°C. Conventional carbonization, i.e., slow pyrolysis,
89produces biochar as the major product along with a small amount of syngas including CO, CH₄,
90and H₂, and condensed bio-oil (Liu et al., 2015b). It requires a relatively long residence time (> 1
91h) and low heating rate (5-7°C/min). Comparatively, fast pyrolysis favours the production of bio-
92oil, of which the heating rate is over 200°C/min and the residence time is less than 10 s (Qian et
93al., 2015). The solid residue, i.e., biochar, may display relatively small surface area due to
94incomplete pyrolysis and tar-like materials entrapped in the pores (Lobos et al., 2016).
95Gasification is the thermochemical process that produces biochar as the solid co-product and
96syngas as the main product at > 700°C in the presence of oxidizing agent (O₂ or steam). Tar
97reforming that shares a similar operation mechanism also gives biochar as a secondary product.
98Hydrothermal carbonization of biomass resulted in hydrochar as the biochar analogue at low
99temperatures (180-250°C) under pressure in water, which eliminates the energy-intensive drying
100of feedstock (Libra et al., 2011). It therefore appears as a cost-effective approach to generate
101biochar for catalytic applications.

1022.1.1 Feedstock

103Biomass with varying contents of hemicellulose, cellulose, and lignin may yield biochars with
104distinctive physicochemical properties under the same temperature (Keiluweit et al., 2010). This

105 is because the three types of polysaccharides show different thermal liability, e.g., hemicellulose,
106 cellulose, and lignin decomposes at 220-315°C, 315-400°C, and 160-900°C, respectively, as a
107 result of their difference in structural features such as crystallinity, cross linking, and branching
108 (Yang et al., 2007; Keiluweit et al., 2010). Therefore, the composition of biomass feedstock may
109 determine the heating temperature required to obtain the desirable porous structure. For example,
110 the microcrystalline cellulose without lignin gave graphitic structure at 350°C, which was much
111 lower than the temperature of 700-900°C employed for lignocellulosic biomass (Lobos et al.,
112 2016). The matrix of raw biomass also affects the biochar micro-structure. For instance, wood
113 biochar showed intricate network of fibrous ridged surfaces, pores, and channels resembling the
114 structure of raw wood, which vastly differed from the planar structure of the sugar-derived carbon
115 (Dehkhoda et al., 2010; Dong et al., 2015).

116 Ash content in the feedstock is important for the biochar properties and catalytic performance.
117 Inorganic elements (Ca, K, Na, P, Si, Mg) were concentrated in the char after pyrolysis, which
118 may play as the active sites for catalysis of, for example, methane decomposition (Klinghoffer et
119 al., 2015) and hydrogen production (Yao et al., 2016) (**Section 4.2**). Therefore, it is important to
120 select appropriate feedstock for the corresponding application, modulating the extent of biochar
121 modification or even dispensing with it. Nevertheless, high ash content in biomass feedstock
122 could retard the formation of stable polycyclic aromatic carbon (SPAC) fraction that determined
123 the biochar stability (McBeath et al., 2015). In particular, high concentration of Si would affect
124 the efficiency of metal impregnation (a type of modification; **Section 2.2**) because it promoted
125 metal sintering upon melting at high temperature and reduced the degree of metal dispersion (Yao
126 et al., 2016).

127 2.1.2 *Temperature*

128 The temperature of the thermochemical treatment is critical for the biochar properties. In general,
129 the fixed carbon content, surface area, and pore volume increase with the temperature as more

130volatile matters are released from the biomass, despite the reduction of biochar yield as a trade-
131off (Yuan et al., 2013; McBeath et al., 2015; Lobos et al., 2016). As the temperature rises, the
132microcrystalline cellulose in biomass gradually transforms in five phases: unaltered material,
133transition char, amorphous char, composite char, and turbostratic char (Keiluweit et al. 2010).
134The last stage is achieved at 600-700°C. Such transformation is associated with the gradual loss
135of oxygen functional groups and aliphatic groups such as cutans and lipids (400°C), as well as the
136formation of polycyclic aromatic structures via dehydration reactions (Keiluweit et al. 2010;
137McBeath et al., 2015). The temperatures of 500-700°C were revealed as the optimal in terms of
138the SPAC content and biochar yield for the commonly used feedstock (e.g., wood,
139agricultural/forestry residue, manure, and macroalgae). At higher temperature, condensation of
140volatiles may block the pores, and gasification of char may lead to increased macropore volume
141at the expense of the microporosity (Muradov et al., 2012).

1422.2 *Activation of biochar*

143A wide range of activation methods were used to modify the biochar properties and
144functionalities, such as chemical treatment, gas activation, and metal impregnation, which can be
145conducted before, during, or after biochar synthesis (**Table 1**).

1462.2.1 *Pre-synthesis treatment*

1475.3.1.1 Metal impregnation

148Metal impregnation aims to attach metals as the active sites on biochar, such as Lewis acid sites
149that facilitate glucose isomerization as well as fructose dehydration for HMF/levulinic acid
150production (Liu et al., 2015a; Yu et al., 2016; **Section 3**). This can be achieved by co-calcination
151of biomass with metal compounds. For example, the mixture of pre-hydrolyzed corncob
152comprising sugars and solid residue, and Sn(OH)₄ and Co(OH)₂ were carbonized in a tube-
153carbide furnace under N₂ in two stages (i.e., 100°C for 10 h and 200°C for 38 h) (Liu et al., 2015a;
154**Table 1**). The resultant catalyst had the surface area of 6.34 m²/g, pore volume of 0.003 cm³/g,

155and acid density of 0.542 mmol/g. Metallic Ni as a common catalyst can be loaded in a similar
156manner. Biomass was impregnated with $\text{Ni}(\text{NO}_3)_2 \cdot 6\text{H}_2\text{O}$ solution and subsequently pyrolyzed at
157700°C in N_2 after drying (Shen and Yoshikawa, 2014). Treating the Ni-containing biomass with a
158strong reducing agent, i.e., NaBH_4 , before pyrolysis further enhanced the catalytic performance
159(for tar reforming; **Section 4.2.1**), because the formation of active metallic Ni^0 from cation was
160effectively promoted. Besides, the hydrolysis of NaBH_4 in the Ni^{2+} solution facilitated the
161development of porosity and surface area in biochar. Metal impregnation can be also achieved in
162a post-synthesis manner, which will be discussed in **Section 2.2.2.2**.

1635.3.1.2 Phosphoric acid treatment

164Phosphoric acid treatment of raw biomass could enhance the physical properties of biochar. The
165microcrystalline cellulose was treated with 5% H_3PO_4 at 70-80°C for 2 h under stirring prior to
166pyrolysis (Lobos et al., 2016; **Table 1**). This could increase the surface area from 199 to 557 m^2/g
167(electroactive surface area: from 18 to 38 m^2/g) and pore volume from 0.026 to 0.22 cm^3/g as a
168result of H_3PO_4 -mediated dehydration of the cellulose. More structural defects such as terraces,
169steps, and kinks were also created on the surface to benefit the subsequent metal impregnation
170step, resulting in the catalyst with electrocatalytic activity four times higher than that without
171 H_3PO_4 treatment. Such acid treatment also favoured the formation of biochar over liquid products
172during fast pyrolysis. Similar observations were remarked in another recent study, which
173demonstrated the activation of raw biomass via H_3PO_4 pretreatment followed by carbonization
174under steam/ N_2 mixture (Shen et al., 2015a). This biochar possessed high surface area (1955
175 m^2/g) and porosity (0.48 ml/g), which may favour homogeneous dispersion of metals (Mn-CeO_x)
176during the subsequent impregnation, compared to the post-pyrolysis steam-activated biochar and
177activated carbon.

1782.2.2 *Post-synthesis treatment*

1795.3.1.3 Sulfonation

180Sulfonated biochar is an effective catalyst for acid-driven reactions. Not only the strong sulfonic
181acid groups are introduced, but the weak acid groups are also created including carboxyl and
182phenolic hydroxyl groups (Kastner et al., 2012; Deng et al., 2016). They can serve as the
183Brønsted acid sites to catalyze hydrolysis and dehydration process (Osatiashtiani et al., 2014; Yu
184et al., 2016; **Section 3**), as well as esterification and transesterification (Dehkhoda et al., 2010;
185**Section 4.1.1**). In addition, H₂SO₄ can enlarge the surface area and pore structure of biochar that
186are conducive to better catalytic performances in general (Kastner et al., 2012). Yet, the opposite
187may occur under excessive sulfonation, for example, up to 98% decrease in surface area as
188reported in the literature (Dehkhoda et al., 2010).

189Typical sulfonation reagents include concentrated sulphuric acid (~98%), fuming sulphuric acid,
190and gaseous SO₃. It was reported that biochar modified by concentrated sulphuric acid showed a
191lower catalytic activity for transesterification (**Section 4.1.1**) in comparison to that sulfonated by
192fuming sulphuric acid (Dehkhoda et al., 2010). Another study also suggested that the
193concentrated acid-sulfonated biochar (99% H₂SO₄) displayed lower –SO₃H group density than the
194gaseous SO₃-sulfonated carbons as the SO₃ gas was more reactive and selective (Kastner et al.,
1952012). Moreover, the former carried weaker acids as the hydrogen bonding sites, which promoted
196water adsorption on the catalyst that hindered the catalytic activity for esterification.

197There is a high potential of sulfonated biochar in wider applications such as organic chemical
198synthesis. Acetanilide, N-butylacetamide, and nitroacetanilide can be produced via the N-, O-,
199and S- acylation processes over the sulfonated amorphous carbon-silica composite (Gupta and
200Paul, 2011). The latter may be replaced by sulfonated biochar that shares the same active sites.

2015.3.1.4 Metal impregnation

202Incipient wetness impregnation is a common technique to load metal nanoparticles on the biochar
203support. The Ni-containing biochar (for catalytic hydrogen production) was produced by
204immersion in the aqueous solution of Ni(NO₃)₂·6H₂O for 4 h, followed by drying and calcination

205at 800°C (Yao et al., 2016). Similarly, Ni-based biochar was produced for catalytic tar conversion
206(Shen and Yoshikawa, 2014). It is interesting to note that biochar impregnated before pyrolysis
207(**Section 2.2.1.1**) showed higher tar conversion efficiency than the one impregnated after
208pyrolysis, possibly due to the higher surface area of the former (135-218 vs 62-87 m²/g). For iron
209nanoparticles, impregnation was conducted with iron nitrate solution followed by 1-h calcination
210at 1000°C (for syngas conversion; Yan et al., 2013) or 300°C (for tar reforming; Kastner et al.,
2112015), which may result in metallic iron and iron carbide as the major species. The metal
212particles were effectively anchored upon the decomposition of surface oxygen functional groups
213during impregnation. The synergy between stable carbonaceous shell and strong iron core
214prevented the sintering of metals and collapse of catalyst structure during application.

215Platinum, ruthenium, and copper particles can be loaded in a similar manner. The biochar
216dispersed in the buffer solution (pH 3) containing CuSO₄ and RuCl₃ was sonicated for 30 min,
217followed by the addition of the reducing agent NaBH₄ to yield Cu-Ru nanoparticles (Lobos et al.,
2182016). The intermediate product was further dispersed in the H₂PtCl₆ solution to give the Cu-
219Ru@Pt core-shell nanoparticles on biochar, which exhibited high catalytic activity for electro-
220oxidation of methanol (**Section 4.3.1**). For synthesis of catalyst containing Pt only, the last step
221using H₂PtCl₆ solution was appropriate (Fan et al., 2015). It is noteworthy that calcination was not
222required in these protocols (Fan et al., 2015; Lobos et al., 2016). Nevertheless, metal
223impregnation may partially block the pores according to a recent study on biochar-supported Mn-
224CeO_x (Shen et al., 2015a).

225Sol-gel method is an alternative metal impregnation technique for synthesis of TiO₂-loaded
226biochar. This process involves the sequential addition of TiO₂ precursor (e.g., titanium
227isopropoxide and tetrabutylorthotitanate), ethanol, and other additives (e.g., diethanolamine and
228HCl), with calcination serving as the last step (Li et al., 2007; Kim and Kan, 2016). The
229calcination temperature ranging from 300-700°C may exert marginal effect on the surface area

230(237-293 m²/g) (Li et al., 2007). The resultant biochar/TiO₂ catalyst was shown effective for
231photocatalytic degradation of antibiotics (Kim and Kan, 2016) and dye (Li et al., 2007) (**Section**
2325.2).

233The application of metal-impregnated biochar may extend to chemical production from biomass
234in a way similar to other carbonaceous materials, such as Ni/Zn-activated carbon catalysts for the
235conversion of cellulose to lactic acid (Zhang et al., 2011b) and Ru-mesoporous carbon catalysts
236for the hydrolysis of cellulose to glucose (Kobayashi et al., 2010).

2375.3.1.5 Gas activation

238Biochar can be activated via steam treatment under heating (700-850°C, 1-7 h) (Cha et al., 2010;
239Iwazaki et al., 2010; Shen et al., 2015a; Rajapaksha et al., 2016b). Steam activation successfully
240increased the surface area of silk biochar by 122-196 times and enlarged the mesopore volume
241for efficient mass transport during catalytic application, with minor effect on surface morphology
242(Iwazaki et al., 2010). Compared to the commercial activated carbon, the steam-activated cotton
243biochar showed a comparable surface area (496 and 516 m²/g) but lower pore volume (0.27 vs
2440.08 ml/g) after metal impregnation (Shen et al., 2015a). It was outcompeted by the biochar co-
245activated by H₃PO₄ and steam, which exhibited the outstanding surface area of 1955 m²/g and
246large pore volume of 0.48 ml/g (**Table 1**). In general, the steam-activated biochar did not perform
247as well as the commercial catalysts (e.g., Pt/C catalyst for oxygen reduction reaction; Iwazaki et
248al., 2010; **Section 4.3.2**) or biochar activated by acid/base (e.g., H₃PO₄/steam- and KOH-activated
249biochar for NO conversion; Cha et al., 2010; Shen et al., 2015a; **Section 5.1**).

250It has been reported that CO₂ treatment coupled with heating (850°C, 15 min) significantly
251increased the surface area of duckweed biochar from 5-12 to 60 m²/g (Muradov et al., 2012).
252Such treatment also enhanced the microporosity by creating new pores via CO₂ gasification
253reaction, while the pore structure remained nearly unchanged. Apart from activation, CO₂ was
254also employed for supercritical drying of aerocellulose precursors before pyrolysis to ensure the

255 nanostructure of the pyrolytic carbon (Guilminot et al., 2008). This may apply to biochar
256 production for preserving the original (or pre-modified) structure of the biomass feedstock.

257 Ozone treatment of biochar (23°C, 6 h) can introduce weak acidic groups on the surface, for
258 example, carboxylic, phenolic, and lactonic groups (Kastner et al., 2012). However, these weak
259 acids neither promoted esterification nor assisted the strong $-\text{SO}_3\text{H}$ groups in a synergistic
260 manner.

261 5.3.1.6 Base treatment and ionic liquid grafting

262 Treatment with base such as KOH has been commonly adopted to increase the surface area and
263 porosity of biochar (Dehkhoda et al., 2010; Jin et al., 2014; Fan et al., 2015). The activation of
264 rice straw and sewage sludge derived biochar in KOH (KOH:biochar = 1:1, 60°C, 2 h) followed
265 by calcination (700°C, 1 h) successfully expanded the surface area from 140 to 772 m^2/g and from
266 18 to 783 m^2/g , respectively, in association with the increased pore volume (Cha et al., 2010).
267 Such results also indicated the feedstock-dependent efficiency of chemical activation. The
268 ultrasound-assisted KOH treatment may further enhance the properties according to an earlier
269 study, which demonstrated significant increase in the surface area (from 16.7 to 702 m^2/g) and
270 pore volume (from 0.01 to 0.39 cc/g) of switch grass biochar (Bhandari et al., 2014). The
271 improvement may be ascribed to the ability of KOH to facilitate hydrolysis reaction on the
272 biochar surface and dissociation of tar-like materials entrapped in the pores (Lin et al., 2012).

273 An innovative surface modification using ionic liquid has been recently reported to produce
274 biochar catalyst for HMF production (Zhang et al., 2017). The ionic liquid was grafted on the
275 sulfonated biochar first. The chloride from the ionic liquid was then substituted by fluorine via
276 ionic exchange using F-containing acids. Such modification improved the substrate accessibility
277 to $-\text{SO}_3\text{H}$ sites by loosening the carbon sheets, and augmented the acidity and thermal stability of
278 the $-\text{SO}_3\text{H}$ groups via the intramolecular electrostatic interaction with the ionic liquid (Zhang et
279 al., 2017).

2803. **Emerging applications of biochar-based catalysts for chemicals production**

2813.1 *Pathways of catalytic biomass conversion into versatile chemicals*

282 Lignocellulosic biomass is a renewable raw material for synthesis of various platform chemicals
283 and biofuels (**Fig. 1**). It comprises carbohydrate polymers (cellulose and hemicellulose) and
284 aromatic polymers (lignin) interacting via intra- and inter-molecular hydrogen bonds.
285 Valorization of these biopolymers involves extensive breakdown and transformation reactions,
286 among which hydrolysis, isomerisation, dehydration, and rehydration have been demonstrated to
287 be facile over biochar-based catalysts.

288 Hydrolysis involves the breakage of glycosidic bonds in polysaccharides to release
289 monosaccharides, for example, converting xylan and glucan to xylose and glucose, respectively.
290 In general, the hydrolysis of lignocellulosic biomass is initiated by Brønsted acid (proton) at the
291 temperature range of 90-260°C under atmospheric or pressurized conditions (Zhou et al., 2011).
292 Proton attacks the oxygen atom in glycosidic linkages to form a cyclic carbonium ion, which
293 subsequently accepts a hydroxide ion to yield the monosaccharide (Zhou et al., 2011; Zhang et
294 al., 2016). Lewis acid (electron pair acceptor) may also weaken glycosidic bond by coordinating
295 with the glycosidic oxygen in a similar fashion (Tao et al., 2011).

296 The released monomeric aldoses (glucose and xylose) can be isomerized into ketoses (fructose
297 and xylulose, respectively), of which the carbonyl functional groups (C=O) exhibit higher
298 reactivity to facilitate further reactions for upgrading. Activation barrier for the dehydration of
299 glucose and xylose are higher than that of fructose and xylulose, respectively (Choudhary et al.,
300 2012; Enslow and Bell, 2015), due to the stable ring structure of aldoses. Isomerization usually
301 occurs at the temperature ranges of 90-110°C over Lewis acid or Brønsted base catalysts, which
302 promotes the critical hydrogen transfer from C2 to C1 (Zhang et al., 2016).

303 Fructose and xylulose undergo dehydration to produce HMF and furfural, respectively. The

304process is mediated by Brønsted acid catalyst at a temperature range of 120-200°C (Zhang et al.,
3052016). These chemicals containing a furan ring, aldehyde group, and alcohol group (in HMF) are
306high-value precursors of medicines, polymers, and biofuels, which could substitute the petrol-
307derived commodities as well as relieve the stress on fossil energy and burden of greenhouse gas
308emissions. Levulinic acid and formic acid as the products of the acid-catalyzed rehydration of
309HMF are also versatile platform chemicals.

310Polymerization as an irreversible side reaction becomes significant at high temperatures and
311prolonged reaction time during the catalytic conversion (Chen et al., 2017b; Yu et al., 2017a). It
312occurs among the substrates, intermediates, and products to form the carbonaceous humins,
313which lowers the yield and selectivity of desirable products. In case of heterogeneous catalysis,
314humins may block the active sites and hence undermine the performance of solid catalyst after
315repeated use (Deng et al., 2016; Chen et al., 2017a). Previous studies suggested that both
316Brønsted acid and Lewis acid play a role in promoting polymerization, depending on the acid
317strength and acid site number (Li et al., 2016; Tsilomelekis et al., 2016; Yu and Tsang, 2017).
318Therefore, active sites and Brønsted-to-Lewis acid ratio of biochar-based catalyst should be
319carefully designed to strike a balance between promoting the desired pathways and the
320unavoidable side reactions.

321Other reactions including epimerization of xylose to lyxose and glucose to mannose,
322retroaldolization of fructose to glyceraldehyde and dihydroxyacetone, as well as glucose to
323glycolaldehyde and erythrose would take place simultaneously during the HMF or furfural
324production (Zhang et al., 2016). However, these pathways are not covered in this review because
325they have not yet been demonstrated over biochar-based catalysts to our best knowledge.

3263.2 *Biochar catalyst for biomass valorization into chemicals*

3273.2.1 *Biochar catalyst for hydrolysis*

328In the presence of sulfonated corn stover-derived biochar, the lignocellulosic biomass, i.e., corn

329stover, switch grass, and prairie cord grass, yielded glucose of 8-10% (19-22% conversion) and
330xylose of 23-41% (68-81% conversion) with respect to the corresponding polysaccharide (Li et
331al., 2013; **Table 2**). The results were comparable to the hydrolysis of model compounds over the
332same catalyst: cellulose gave 3% glucose (24% conversion) and xylan produced 40% xylose
333(100% conversion). This demonstrated that the biochar-based catalyst maintained high
334performance confronting the impurities and complex matrix in biomass. A similar conversion of
33585% of model xylan was achieved using sulfonated biochar derived from wood and peanut hulls
336(Ormsby et al., 2012; **Table 2**). Interestingly, this biochar had greater surface area (365 vs 10 m²/
337g), larger pore volume (0.2 vs 0.05 cm³/g), and higher acid density (3.66 vs 0.95 mmol/g)
338compared to the abovementioned corn stover biochar, while the density of –SO₃H group as the
339strong Brønsted acid in both catalysts are 0.7. This comparison implies that the strong active sites
340may play an important role besides the total acidity, surface area, and pore volume.

341The biochar catalyst showed faster xylan hydrolysis rates than the commercial sulfonated
342macroreticular resin (Amberlyst 15) at 90-110°C, with the turnover frequency (TOF) 15 times
343higher (Ormsby et al., 2012). Although the acid density of Amberlyst 15 was much higher than
344the biochar catalyst (4.71 vs 0.69 mmol/g), its far smaller surface area and pore volume restricted
345the accessibility to active sites as well as adsorption capacity for the substrates. Therefore, we
346may expect a threshold for these physical parameters, below which the accessibility and contact
347between substrate and catalytic site appears as the limiting factor regardless of the acid site
348density. Apart from improving the surface area and porosity, it is also desirable to manipulate the
349position of active sites (i.e., within mesopores or on the exterior surface) via surface modification
350for managing the catalytic reactions in biochar. Nevertheless, the difference in hydrolysis rates
351became less apparent when the temperature increased to 120°C (Ormsby et al., 2012), probably
352due to the enhanced mass transfer. Higher energy input also favoured the kinetics of xylan
353hydrolysis (2 h at 120°C vs 24 h at 93°C to obtain ~90% xylan conversion). Likewise, for

354cellulose hydrolysis, high temperature of 275°C allowed 100% conversion of cellulose within a
355short reaction time of 15 min over a sulfonated biochar catalyst in methanol as the medium (Dora
356et al., 2012).

357Biochar exhibited significantly higher hydrolysis activity than activated carbon in terms of xylan
358conversion (85 vs 57%), initial reaction rate (30 times), and TOF (9 times) at the same
359temperature, despite its lower surface area (365 vs 1391 m²/g) (Ormsby et al., 2012). This was
360because the activated carbon may not be effectively sulfonated due to the considerable cross
361linking and polymerization as a result of energy-intensive activation process (900-1000°C). In
362addition, while the micro-/mesopores harboured the acid sites within activated carbon, the acid
363groups on the biochar surface were more accessible to the large substrates such as cellulose and
364hemicellulose (Li et al., 2013). Besides, the hydrophobicity of biochar prevented the sulfonic
365groups from hydration, upon which they were easily leached as sulphuric acids in the aqueous
366system (Li et al., 2013; Gallo et al., 2016).

367The recyclability of biochar-based catalyst should be considered. It was reported that the catalytic
368activity of reused sulfonated biochar declined by ~14% in the second run, and it was completely
369deactivated after the fourth run due to acid site leaching and mass loss (Ormsby et al., 2012).
370Comparatively, the mesoporous carbon-supported Ru nanoparticles maintained steady cellulose
371hydrolysis (20-21% glucose) over five runs, during which metal leaching was not detected
372(Komanoya et al., 2011). Therefore, metal impregnation may be a viable alternative to
373sulfonation to modify biochar for catalytic hydrolysis of glucans (glucose-based polymers).

3743.2.2 *Biochar catalyst for isomerization and dehydration*

375Functionalized biochar are also able to facilitate isomerization of glucose to fructose and/or
376dehydration of glucose to HMF. Biochar-based sulfonic acids modified by ionic liquid achieved
377HMF yield of 27.94% from cellulose with a moderate selectivity of 62% within 3 h at 80°C in
378water (Zhang et al., 2017; **Table 2**). The promising performance was ascribed to the grafted ionic

379liquid that enhanced the accessibility, acidity, and thermal stability of $-\text{SO}_3\text{H}$ sites. The
380performance may be improved by changing the solvent. For example, 65% HMF at maximum
381was yielded from inulin (a glucan) in ionic liquid at 100°C for 60 min over the model lignin-
382derived sulfonated hydrochar, of which the performance was competitive with the common solid
383catalysts (e.g., Amberlyst and sulphated zirconia) (Kang et al., 2013). Similarly, sulfonated
384biochar achieved a furfural yield of 81.1% (83% selectivity) from the pre-hydrolyzed corncob at
385 170°C in 60 min under the biphasic co-solvent (Deng et al., 2016; **Table 2**). The latter system
386allowed rapid and continuous extraction of furfural to the organic phase upon production in the
387aqueous phase, reducing the off-path humins formation for high furfural yield. The reclaimed
388biochar catalyst (subsequently washed by hot water, ethanol, and acetone) showed a decrease in
389the furfural yield from 81 to 24.6% after five runs, which was associated with 91.4% reduction in
390the $-\text{SO}_3\text{H}$ group density and 94% increase in the humins-to-catalyst ratio. Thus, regeneration of
391the catalyst at 150°C in sulphuric acid (98%) was required after each run to maintain the
392performance.

393Besides sulfonated biochar, mineral-impregnated ($\text{SnO}_2\text{-Co}_3\text{O}_4$) biochar catalyst yielded 30% of
394furfural from corncob in water at maximum (Liu et al., 2015a). The multivalent metal functioned
395as Lewis acid sites to facilitate the isomerization of xylose to the more reactive xylulose for facile
396dehydration reaction afterwards. The metals also reacted with hydroxyl ion from water to
397generate Brønsted acid density (0.538 mmol/g), promoting the hydrolysis of glycosidic bond as
398well as dehydration of xylulose. Therefore, the Brønsted acid and Lewis acid facilitated the
399tandem reactions in a cooperative manner to produce furfural effectively. Similar synergistic
400effect was also remarked for the HMF production from food waste over homogenous metal
401chloride catalysts (Yu et al., 2016; Yu et al., 2017b) as well as from standard glucose over the
402heterogeneous SO_4/ZrO_2 catalyst (Osatiashtiani et al., 2014). In the latter case, Lewis acid sites
403may be assisted by the coexisting Brønsted base to facilitate isomerization, according to the

404mechanistic studies on CrCl₃-mediated glucose transformation (Choudhary et al., 2013a;
405Choudhary et al., 2013b). The basic -OH group in the active species [Cr(H₂O)₅OH]²⁺, which was
406formed upon the partial hydrolysis of Cr³⁺ in water, activated the critical Cr-catalyzed hydride
407shift within glucose by initiating a proton transfer.

408Therefore, introducing both Brønsted and Lewis acidity to biochar by acidification and/or
409mineralization is favourable and pivotal for the catalytic valorization of biomass. The ratio of the
410dual functions is critical for high product yield and selectivity. A recent review has illustrated that
411the optimum Brønsted-to-Lewis acid ratio varies for glucose conversion to HMF over zeolites
412and niobium oxides, depending on the system components such as solvent and temperature (Yu
413and Tsang, 2017). The acid-to-base ratio may also play a role in case of acid- and base-carrying
414bifunctional candidate such as SO₄/ZrO₂ catalyst (Osatiashtiani et al., 2014). In addition, the acid/
415base strength may arise as another important parameter that tunes the system selectivity towards
416the favourable reactions relative to the side reactions, according to the recent studies on model
417compound conversion over mineral catalysts (Kreissl et al., 2016; Li et al., 2016). These
418considerations should be taken into account when tailoring the active sites on biochar-based
419catalysts.

420Pore structure that determines the accessibility for substrate to the active catalytic sites should
421also be carefully designed. Sulfonated carbons with hierarchically ordered macropores (220 nm)
422and mesopores (4.8 nm) (SCHOP) synthesized using a template showed significantly higher
423fructose conversion (100%) than the regular mesopore (71.9%) and micropore (52.4%)
424sulfonated carbons within 18 min (Wang et al., 2016). Contrasting with the surface catalysis on
425micro- and mesoporous carbon, SCHOP enabled diffusion within the macro-channels, favouring
426contact between fructose and internal active sites as well as separation of products from the active
427sites. The authors also proposed the hierarchically ordered pore structure enhanced the resistance
428of active sites against blocking by humins, although the mechanism was not elucidated.

429 Interestingly, acidic mesoporous carbon (CMK-5) with a smaller pore size (2.67 & 3.38 nm vs
430 7.5 nm) and lesser acid sites (0.9 vs 2.3 mmol/g) gave a higher TOF of 0.069 min⁻¹ for fructose
431 dehydration to HMF, compared to the silica-based catalyst (TOF = 0.048 min⁻¹) (Crisci et al.,
432 2010; Gallo et al., 2016). We infer that the better performance and low deactivation rate of CMK-
433 5 may pertain to its higher surface area (616 vs 218 m²/g) and bimodal pore structure. These
434 findings may highlight the significance of porous structure and location of catalytic sites of
435 biochar for sustainable biomass valorization processes.

436 3.2.3 Biochar catalyst for rehydration

437 Levulinic acid (LA) is also a key platform chemical of polymers and fuels. There is no study on
438 the production of LA over biochar-based catalysts to our best knowledge. However, a great
439 potential is anticipated as mineral acids (e.g., HCl, H₂SO₄, H₃PO₄), solid acid, inorganic salts
440 (e.g., FeCl₃), and zeolite have been demonstrated as effective catalysts to give promising yield of
441 LA (Morone et al., 2015; Wei and Wu, 2017; Chen et al., 2017b). Modification towards these
442 functionalities could realize the application of biochar for facile LA production from biomass. It
443 was reported that LA was detected as a by-product under prolonged reaction time and increased
444 temperature during biomass valorization mediated by functionalized biochar (Zhang et al., 2017).

445 4. Emerging application of biochar-based catalysts for energy production

446 4.1 Bio-oil production

447 4.1.1 Esterification/ transesterification

448 Biochar-based catalysts have been applied for biodiesel production. The free fatty acid (FFA),
449 from vegetable oil and animal fats, and low-molecular-weight alcohol undergo esterification to
450 give esters as the biofuel (**Fig. 2**). Sulfonated biochar maintained high FFA conversion of 97-98%
451 from refined microalgal oil in methanol for three runs at 100°C (Dong et al., 2015; **Table 3A**).
452 Using waste vegetable oil as the FFA source, 77-89% FFA conversion can be achieved over an
453 analogous sulfonated biochar at 60°C in the presence of ethanol (Dehkhoda et al., 2010). These

454 results are comparable to the esterification of model FFAs, for example, 70-100% conversion of
455 pure palmitic and stearic acids at 55-60°C, depending on the amount of methanol (Kastner et al.
456 2012). This strongly evidenced the applicability of biochar catalyst for biofuel production via
457 esterification. However, significant chlorophyll and phospholipids in particular biomass, e.g.,
458 microalgae, may inhibit the catalyst and lower the biodiesel quality, which should be removed
459 upfront (Dong et al., 2015; **Table 3A**).

460 In comparison to the commercial Amberlyst 15, biochar achieved a higher conversion of FFA
461 from microalgal oil (99 vs 94%) under the same reaction condition, which may be attributed to
462 the better dispersion of biochar in the medium (Dong et al., 2015). Another study showed that
463 after sulfonation (99% H₂SO₄), the activated carbon exhibited higher esterification activity than
464 the biochar catalysts (97 vs 70% conversion) due to the larger pore volume (0.76 vs 0.13-0.2 cm³/
465 g) and pore radius (1.1 vs ~1.06 nm) (Kastner et al. 2012). These favourable properties facilitated
466 the access of the substrates to the active sites, which may compensate for the shortcomings of
467 lower –SO₃H density in the activated carbon (0.2 vs 0.61-0.69 mmol/g).

468 Biochar catalyst also applies to transesterification, during which glyceride in vegetable oil and
469 animal fat reacts with low-molecular-weight alcohol to produce esters (biodiesel) and glycerol.
470 The process shows a higher dependence than esterification on strong Brønsted acidity. Fuming
471 H₂SO₄-modified biochar that possessed more –SO₃H groups (~1 mmol/g) gave noticeable
472 amounts of products, i.e., 47-64% methyl oleate and 13-20% methyl linoleate from canola oil and
473 methanol, equivalent to a maximum biodiesel yield of 10% (Dehkhoda et al., 2010; **Table 3A**). It
474 can be also observed that the production increased as a function of the surface area of catalyst. In
475 contrast, the hydrothermally sulfonated biochar using concentrated H₂SO₄ did not catalyze
476 transesterification probably due to the relatively low content of –SO₃H sites (~0.6 mmol/g)
477 (Dehkhoda et al., 2010). However, using the hydrothermally sulfonated biochar, Dong et al.
478 (2015) reported about 5% higher yield of fatty acid methyl ester (FAME) from microalgal oil at

479 120°C compared to 100°C. This suggested that the transesterification activity can be increased by
480 energy supply, which may pertain to the enhanced miscibility of triglyceride in methanol at high
481 temperatures.

482 It was demonstrated that after pre-esterification of microalgal oil by sulfonated biochar, CaO was
483 added for the subsequent transesterification, attaining 99% FAME yield (Dong et al., 2015). It is
484 more sustainable to apply CaO-containing biochar derived from CaCO₃-rich biomass, e.g., palm
485 kernel shell. The latter can achieve nearly 100% FAME production under optimal conditions
486 according to an optimization and kinetic study (Kostić et al., 2016). Other Ca-rich waste
487 materials such as waste egg shell (Chakraborty et al., 2010), bovine bone waste (Smith et al.,
488 2013), and crab shell (Madhu et al., 2016) may be considered as additives to biomass feedstock
489 for co-pyrolysis, manufacturing cost-effective transesterification biochar-based catalyst (Chen et
490 al., 2017a).

491 4.1.2 Hydrogenation

492 Syngas derived from thermochemical conversion of biomass contains CO, H₂, CO₂, and volatile
493 hydrocarbons, which can be upgraded into fuels through different processes. The biochar-based
494 carbon-encapsulated iron nanoparticle catalyst promoted Fischer-Tropsch synthesis (FTS)
495 effectively, achieving 95% CO conversion and 68% liquid hydrocarbons selectivity (Yan et al.,
496 2013; **Table 3B**). Besides, activated biochar loaded with ruthenium facilitated methanation, in
497 which 97% CO and 55% CO₂ in syngas were converted to give a CH₄ yield of 54% (92%
498 selectivity) under sufficient H₂ supplement (Wang et al., 2014). The large surface area (728-757
499 m²/g) of activated biochar favoured a higher dispersity of Ru (> 70%) compared to other
500 conventional support such as Al₂O₃ (43%) and SiO₂ (17%), which may account for the effective
501 catalytic performance.

502 In addition to syngas conversion, the application of modified biochar may extend to other

503chemical synthesis that involves hydrogenation. For example, coconut shell activated carbon
504incorporated with Pd-Ni-B amorphous alloy achieved nearly 100% conversion of the
505nitroaromatic compounds (Chen et al., 2015). This illustrates the great potential of metal-
506impregnated biochar as a solid catalyst for other analogous industrial processes.

5074.2 *Biogas production*

5084.2.1 *Tar reforming*

509Tar reforming is referred to turning the hydrocarbon mixture (e.g., phenolic, olefin, and
510polycyclic aromatic compounds) that is unavoidably formed during biomass gasification and
511pyrolysis into valuable syngas. Biochar containing catalytic sites in common with the
512conventional catalysts could be effective for tar reforming, including dolomites (calcium
513magnesium carbonate), olivine (magnesium iron silicate), and nickel- and alkali metal-based
514catalysts (Anis and Zainal, 2011). A recent study showed that 95% removal of the alkali and
515alkaline earth metals (Ca, K, Mg, P, and Na) from biochar led to 18% decrease in the
516decomposition of methane, illustrating the significance of these elements for the catalytic tar
517reforming despite their small quantity (2%) (Klinghoffer et al., 2015). Similarly, K- and Ca-
518containing switchgrass biochar achieved high removal efficiency, although their roles were not
519discussed (Bhandari et al., 2014). The switchgrass biochar activated by KOH gave the best
520performance, i.e., about 90% removal of toluene possibly due to the high surface area (~ 900
521 m^2/g) (**Table 4A**). In addition, iron calcined biochar (Kastner et al., 2015) and silica-based nickel
522nanoparticle-embedded biochar (Shen and Yoshikawa, 2014) also proved effective.

523Biochar as the catalyst support was critical. The activity of mineral ash was about 90% lower
524than the biochar-based catalyst, probably due to the inefficient metal dispersion (Klinghoffer et
525al., 2015). The metal dispersion depended on the biochar formation environment, for instance,
526biochar produced from gasification in CO_2 showed higher metal dispersion, while a steam-
527containing atmosphere led to agglomeration of the metal species. The authors also remarked the

528 potential catalytic activity of the carbon support. The basic oxygen groups (carbonylic, quinonic,
529 and pyrone structures) might play an important role as they remained attached at the cracking
530 temperature of 700-900°C, while acidic groups (lactones or carboxylic groups) underwent
531 desorption at 350°C.

532 As the reforming process prolonged, ring condensation in the biochar resulted in loss of oxygen
533 functional groups as well as relocation and agglomeration of the metal species, of which the
534 dispersion and catalytic activity decreased (Min et al., 2013). Another cause of catalyst
535 deactivation was the coke deposition on biochar associated with pore blockage and surface area
536 reduction (Bhandari et al., 2014; Shen and Yoshikawa, 2014), which is similar to the adverse
537 impact of humins on biomass conversion to chemicals (**Section 3**). Nevertheless, compared to the
538 conventional tar reforming techniques (dry/wet gas cleaning, thermal cracking, and plasma
539 cracking) (Anis and Zainal, 2011), catalytic cracking over biochar presents a more cost-effective
540 and green option due to the lower energy consumption. It deserves more research efforts to
541 develop resilience against the undesirable reactions that deactivate the catalyst.

542 4.2.2 Hydrogen production

543 Hydrogen is another sustainable alternative to fossil fuels in view of its low emissions, which can
544 be produced via biogas reforming. Wood biochar achieved 70% CH₄ conversion within 120 ms at
545 1000°C in the presence of CO₂ and steam as the pyrolysis gas (Dufour et al., 2008; **Table 4B**). In
546 such case, biochar was continuously regenerated to maintain high surface area and accessible
547 pore structure via the oxidation of carbon by CO₂ and H₂O at high temperature. Similarly, the
548 CO₂-treated duckweed-derived biochar obtained 82% and 25% conversion of CO₂ and CH₄ at the
549 early stage of biogas reforming, respectively (Muradov et al., 2012). The results outcompeted the
550 untreated biochar (42% and 10% conversion of CO₂ and CH₄, respectively), which had
551 significantly lower surface area compared to the CO₂-treated one (5-12 vs 60 m²/g). Nevertheless,
552 the latter lost its initial activity of ~90% due to blockage of the active sites by carbon deposition.

553It was suggested that the unsaturated carbon atoms, which originated from the thermally
554decomposed surface oxygen functional groups, served as the active sites for the chemisorption
555and decomposition of CH₄ (Dufour et al., 2008). The biochar catalyst gave similar performance
556before and after demineralization in the same study, suggesting the negligible role of ashes for
557promoting methane decomposition. Interestingly, this contrasted the result of methane
558decomposition process for tar reforming (Klinghoffer et al., 2015; **Section 4.2.1**). In addition,
559pyrolytic waste tire biochar achieved 95% conversion of methylcyclohexane to hydrogen upon
560wetness impregnation of Pt nanoparticles in the micro regions (Zhang et al., 2011a), which may
561apply to catalytic methane-to-hydrogen process. More investigations are required to rationalize
562the divergent findings over the active sites on biochar for biogas reforming.

563Biochar enhances the hydrogen production during biomass pyrolysis/gasification. During the
564pyrolysis of microalgae, the addition of unmodified biochar as the catalyst promoted hydrogen
565production and selectivity by the factor of 1.37 and 1.59, respectively (Norouzi et al., 2016).
566Besides, the Ni-loaded biochar catalyst resulted in 64.02 vol% hydrogen in wheat straw
567gasification at 800°C (Yao et al., 2016). The best performing biochar catalyst (derived from
568cotton stalk) contained high contents of K and Ca as revealed by elemental analysis. Similar to tar
569reforming (**Section 4.2.1**), these alkali and alkaline earth metals were significant in promoting
570biomass reforming reactions, possibly through direct catalytic effect and enhanced water
571adsorption (Yao et al., 2016). In contrast, high Si content would result in agglomeration and
572sintering of metals, which reduced the dispersion of catalytic active sites. Other biochar
573properties (external surface area and Ni loading) and gasification conditions (steam-to-biomass
574ratio and temperature) also governed the catalytic performance.

5754.3 *Electrochemical energy utilization*

5764.3.1 *Methanol electro-oxidation*

577Biochar has been also employed for fuel cell production to generate clean and renewable energy.

578 Conventionally, carbon-supported Pt-based electrocatalysts, such as carbon-silica composite
579 aerogels and carbon-supported Pt nanoparticles (Pt/C), are used to promote methanol electro-
580 oxidation in direct methanol fuel cells (Johnson et al., 2011). Biochar-supported Cu-Ru@Pt
581 nanoparticles (derived from acid-treated cellulose) exhibited promising catalytic activity for
582 electro-oxidation of methanol in terms of the high turnover number (TON) of 0.151 molecule
583 (sites s)⁻¹ and a low poisoning rate at 0.026% s⁻¹ (Lobos et al., 2016; **Table 4C**). Its catalytic
584 activity was 3-9 times higher than the commercial Pt-Ru/C catalyst, which was attributed to the
585 electronic and strain effect induced by the interaction between the nanoparticle shells and the
586 highly defective surface of biochar support. The latter (as a result of acid treatment of the biochar
587 precursor, i.e., cellulose) was further highlighted as the key to the fast turnover rate and high
588 poisoning tolerance, which facilitated the oxidation of the poisoning species adsorbed on the
589 nanoparticles. Similarly, the okara-based mesoporous biochar supporting Pt nanoparticles
590 displayed higher electrocatalytic activity than the conventional carbon black-based Pt/C catalyst,
591 generating a higher peak current density (12.2 mA/cm) as well as higher poison resistance (Zhou
592 et al., 2014). The okara biochar showed a high degree of graphitization that favoured the
593 composite conductivity. It also induced abundant grain-interfaces among the loaded Pt particles
594 as the active sites, leading to a higher electrochemical active surface area compared to Pt/C (58.2
595 vs 30.6 m²/g).

596 The KOH-activated pectin hydrochar (hydrothermally carbonized at 200°C for 12 h) was a
597 promising support for Pt nanowires to catalyze methanol electro-oxidation, achieving higher mass
598 current density than Pt/C (450 vs 194 mA/mg) (Fan et al., 2015). The high performance may be
599 related to the preferential exposure of Pt crystal facets and enhanced electron and mass transport
600 at the electrode/electrolyte interfaces. Meanwhile, the surface hydroxyl and carboxyl groups on
601 biochar promoted the formation of hydroxyl species (Pt-OH) in the presence of water, hence
602 accelerating oxidation of poisons such as CO intermediates. Such poison tolerance may resemble
603 the function of defective surface of biochar synthesized from acid-treated cellulose mentioned

604above (Lobos et al., 2016). On the other hand, unmodified hydrochar can also be used as a
605supercapacitor owing to its large specific surface area (2440 m²/g) and balanced micro- and
606mesoporosity that enabled charge accumulation (Fan et al., 2015).

6074.3.2 *Oxygen reduction reaction*

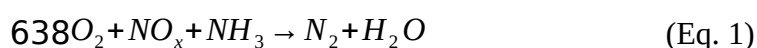
608Steam-activated silk fibroin-derived biochar without metallic elements presented certain
609electrocatalytic activity for oxygen reduction reactions in fuel cell, giving a power density of 142
610mW/cm² (1.42 x 10⁶ mW/m²) operated at 80°C, which was lower than that of the typical Pt/C
611catalyst as the authors remarked (Iwazaki et al., 2010; **Table 4C**). The quaternary nitrogen atoms
612were suggested as the active sites in biochar, while the activity could be further improved by
613incorporating zirconium oxides particles, increasing the average number of electron transferred
614from 3.5 to 3.9.

615Likewise, nanocomposites of iron oxide and biochar (derived from cornstalks and pomelo skins)
616were promising for promoting oxygen reduction reaction in microbial fuel cells (Ma et al., 2014).
617The mixed composites exhibited a power density of 1502 mW/m² at 30°C, which was 26% greater
618than the Pt/C catalyst and was maintained for 18 cycles with small decline (7.12%). The
619uniformly dispersed Fe species on the large surface area (476.5-547.7 m²/g) improved the
620electrical conductivity and density of catalytic active sites. In another study, cellulose-based
621biochar impregnated with Pt showed electrocatalytic activity comparable to Pt/C (-85 to -74 vs -
62279 mV/dec) despite the lower Pt active area due to agglomeration (<10 vs 72 m²/g) (Guilminot et
623al., 2008). Promising results may be obtained by careful selection of the feedstock. For example,
624biochar derived from nitrogen- and iron-rich sludge gave a power density of 500 mW/m² at
625maximum, which was slightly lower than that of Pt/C (625 mW/m²) but greater than bamboo
626biochar (272 mW/m²) and activated carbon (308 mW/m²) (Yuan et al., 2013).

6275. **Emerging application of biochar-based catalysts for pollution control**

6285.1 *NO_x reduction and ammonia ozonation*

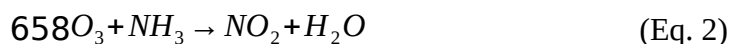
629 Selective catalytic reaction is an effective measure to control NO_x emission, as indicated in Eq. 1.
630 The KOH-activated biochar derived from rice straw and sewage sludge attained 86% and 46%
631 NO_x removal at 50°C, respectively, which was ascribed to the abundance of oxygen functional
632 groups, high surface area, large pore volume, and thus high NH₃ and NO adsorption capacity
633 (Cha et al., 2010; **Table 5**). However, it is interesting to note that the activated rice straw biochar
634 and sewage sludge biochar had comparable surface area (772 and 783 m²/g) and pore volume
635 (0.42 and 0.61 cm³/g), implying that they may not be the most critical factors for high catalytic
636 activity. Instead, the higher content of nitrogen and alkali metals (K and Na) in raw rice straw
637 may make a more significant contribution, which needs further assessment.



639 Transitional metal oxides can enhance the NO_x removal. For instance, impregnating 3 wt% MnO_x
640 to rice straw biochar resulted in an outstanding NO_x removal efficiency of 84% at 50°C (Cha et
641 al., 2010). Similarly, Mn/Ce-impregnated cotton stalk biochar (co-activated by H₃PO₄ and steam)
642 presented higher N₂ selectivity and catalytic activity in comparison to activated carbon and steam-
643 activated biochar (Shen et al., 2015a). This was associated with the favourable physicochemical
644 properties as a result of co-activation process, including specific surface area for catalytic sites
645 (1614 m²/g), surface acidity (71.38 μmol/g), porosity (0.481 ml/g), active site dispersion, metal
646 speciation (Mn⁴⁺/Mn³⁺ = 2.25; Ce⁴⁺/Ce³⁺ >> 1), and surface oxygen functional groups (P-O-C, P-
647 O-P, C=O, C-NO₂, etc.). In particular, the latter two facilitated oxygen transfer and hence the
648 oxidation of NO to NO₂, which improved NO conversion to N₂ via an alternative catalytic
649 pathway.

650 Activated biochar has been applied for catalytic ozonation of gaseous ammonia (Eq. 2), which
651 was produced from pyrolysis of pelletized peanut hulls under steam (Kastner et al., 2009; **Table**
652 **5**). It achieved a high NH₃ conversion of about 65% under the maximum O₃ supply (~900 ppm_v)
653 at 23°C. Carbon surface and water vapour promoted ·OH free radical formation for catalytic
654 ozonation, underscoring the significance of the biochar support. However, at a low O₃

655 concentration (62 ppm_v), its performance was less satisfactory and outcompeted by wood fly ash
656 under the same condition (~18 vs 45% NH₃ conversion), probably due to the relatively low
657 surface area and insufficient active metal oxide species (e.g., Cu, Mn, Ni, and Co).



659 5.2 Photocatalytic degradation of organics

660 Modified biochar is a potential photocatalyst for degradation of organic pollutants. For example,
661 sulfamethoxazole (SMX, antibiotics) can be effectively degraded (91% at maximum) over
662 biochar-supported well-dispersed TiO₂ granules under ultraviolet irradiation, which was prepared
663 by treatment with acid and titanium isopropoxide (Kim and Kan, 2016; **Table 5**). The carbon sites
664 enabled adsorption of SMX via the π-π interaction, while excellent conductivity of carbon
665 suppressed the recombination of electrons and electron holes, which often occurred in the case of
666 commercial TiO₂ lowering the photocatalytic activity. In addition, it was easier to separate the
667 biochar-supported catalyst compared to TiO₂ powder that aggregated after use and required
668 energy-intensive recovery. Likewise, for the removal of methylene blue (MB) as a dye, the
669 vapour-activated coconut shell biochar exhibited higher photocatalytic activity than the TiO₂
670 powder (100 vs 61%) possibly due to favourable adsorption of MB and evenly dispersed TiO₂ on
671 the biochar support, as well as the large surface area (293 m²/g) (Li et al., 2007). These results
672 demonstrated the significance of the accessibility and distribution of catalytic sites, particularly
673 for the metal-mediated processes (e.g., biofuel production in **Section 4**), which could be
674 significantly enhanced by using biochar as the support.

675 Artificial photosynthesis and solar energy conversion may appear as potential applications of
676 biochar-based catalyst upon modification to resemble the structure and photoelectrical properties
677 of nanostructured carbon allotropes (fullerenes, carbon nanotubes, and grapheme), which were
678 effective candidates according to the previous study (Umeyama and Imahori, 2013).

6796. **Prospect**

680In summary, the biochar-based catalyst is promising because of its tuneable surface chemistry and
681porosity that can be engineered to mimic the conventional catalysts. The biochar support exhibits
682intrinsic advantages, e.g., the reserved channel structure and high metal content from particular
683biomass feedstock and abundant carbon-induced interactions with the substrates, which present
684technological merits in addition to sustainability concerns.

685Despite successful demonstration of biochar application as catalysts, there is plenty of room for
686improvement in its catalytic activity and selectivity towards the desirable products. In particular,
687the production of high-value chemicals from biomass is very challenging, of which the
688complexity and recalcitrance often limits the product yield to only 30-40% (**Table 2**).

689Advancement requires the paradigm shift towards “application-oriented” or “reaction-oriented”
690biochar synthesis, as there is no universal conclusion over the most important parameters.

691Therefore, future biochar synthesis should take into account the reaction characteristics upfront
692(e.g., hydrophobicity and molecular size of reactants, intermediates, and products) to inform the
693desirable parameters, thereby designing the production/modification protocol with a bottom-up
694approach.

695We should also reckon the significance of the catalytic site location. For example, when the active
696sites are dispersed within the biochar channels, the pore size governs the catalytic efficiency by
697controlling the reactant diffusion. It exerts trivial impact when the active sites are located on the
698exterior surface. Future investigations are needed to examine the benefits and feasibility of
699impregnating the active sites at designated locations of biochar to control the
700desirable/undesirable reactions for highly efficient and sustainable applications.

7017. **Conclusions**

702Biochar emerges as a sustainable and low-cost catalyst support for chemical synthesis, biofuel
703production, and pollution control, giving performance comparable or superior to

704conventional/commercial catalysts. This review highlights the substrate access to active sites as
705the key to promising catalysis, which counts on the physicochemical properties (-SO₃H density,
706surface area, porosity, metal dispersion, etc.). Their relative significance varies depending on
707where catalysis occurs over biochar, which may be manoeuvred through innovative
708synthesis/modification. By improving the understanding on the effects of existing modifications
709on biochar features, this review advises protocol development to engineer high-performance
710biochar-based catalyst for emerging applications.

7117. Acknowledgement

712The authors appreciate the financial support from the Environment and Conservation Fund (K-
713ZB78) and the Hong Kong International Airport Environmental Fund (K-ZJKC).

714References

7151. Ahmad, M., Rajapaksha, A. U., Lim, J. E., Zhang, M., Bolan, N., Mohan, D., Ok, Y. S., 2014.
716 Biochar as a sorbent for contaminant management in soil and water: a
717 review. *Chemosphere* 99, 19-33.
7182. Anis, S., Zainal, Z. A., 2011. Tar reduction in biomass producer gas via mechanical, catalytic
719 and thermal methods: A review. *Renewable Sustainable Energy Rev.* 15, 2355-2377.
7203. Bhandari, P. N., Kumar, A., Bellmer, D. D., Huhnke, R. L., 2014. Synthesis and evaluation of
721 biochar-derived catalysts for removal of toluene (model tar) from biomass-generated
722 producer gas. *Renewable Energy* 66, 346-353.
7234. Cha, J. S., Choi, J. C., Ko, J. H., Park, Y. K., Park, S. H., Jeong, K. E., Jeon, J. K., 2010. The
724 low-temperature SCR of NO over rice straw and sewage sludge derived char. *Chem. Eng.*
725 *J.* 156, 321-327.
7265. Cha, J. S., Park, S. H., Jung, S. C., Ryu, C., Jeon, J. K., Shin, M. C., Park, Y. K., 2016.
727 Production and utilization of biochar: A review. *J. Ind. Eng. Chem.* 40, 1-15.
7286. Chakraborty, R., Bepari, S., Banerjee, A., 2010. Transesterification of soybean oil catalyzed
729 by fly ash and egg shell derived solid catalysts. *Chem. Eng. J.* 165, 798-805.
7307. Chen, S.S., Maneerung, T., Tsang, D.C.W., Ok, Y.S., Wang, C.H., 2017a. Biomass conversion
731 to hydroxymethylfurfural, levulinic acid, and fatty acid methyl ester by heterogeneous
732 catalysts. *Chem. Eng. J.* in press.
7338. Chen, S.S., Yu, I.K.M., Tsang, D.C.W., Yip, A.C.K., Khan, E., Wang, L., Ok, Y.S., Poon,
734 C.S., 2017b. Valorization of cellulosic food waste into levulinic acid catalyzed by
735 heterogeneous Brønsted acids: Temperature and solvent effects. *Chem. Eng. J.* 327, 328-335.
7369. Chen, T., Li, D., Jiang, H., Xiong, C., 2015. High-performance Pd nanoalloy on
737 functionalized activated carbon for the hydrogenation of nitroaromatic compounds. *Chem.*
738 *Eng. J.* 259, 161-169.
73910. Choudhary, V., Mushrif, S. H., Ho, C., Anderko, A., Nikolakis, V., Marinkovic, N. S.,
740 Vlachos, D. G., 2013a. Insights into the interplay of Lewis and Brønsted acid catalysts in
741 glucose and fructose conversion to 5-(hydroxymethyl) furfural and levulinic acid in aqueous
742 media. *J. Am. Chem. Soc.* 135, 3997-4006.

74311. Choudhary, V., Pinar, A. B., Lobo, R. F., Vlachos, D. G., Sandler, S. I., 2013b. Comparison of
744 homogeneous and heterogeneous catalysts for glucose-to-fructose isomerization in aqueous
745 media. *ChemSusChem*. 6, 2369-2376.
74612. Choudhary, V., Sandler, S.I., Vlachos, D.G., 2012. Conversion of xylose to furfural using
747 Lewis and Brønsted acid catalysts in aqueous media. *ACS Catal.* 2, 2022-2028.
74813. Crisci, A.J., Tucker, M.H., Dumesic, J.A., Scott, S.L., 2010. Bifunctional solid catalysts for
749 the selective conversion of fructose to 5-hydroxymethylfurfural. *Top. Catal.* 53, 1185-1192.
75014. Dehkhoda, A. M., West, A. H., Ellis, N., 2010. Biochar based solid acid catalyst for biodiesel
751 production. *Appl. Catal. A* 382, 197-204.
75215. Deng, A., Lin, Q., Yan, Y., Li, H., Ren, J., Liu, C., Sun, R., 2016. A feasible process for
753 furfural production from the pre-hydrolysis liquor of corncob via biochar catalysts in a new
754 biphasic system. *Bioresour. Technol.* 216, 754-760.
75516. Dong, T., Gao, D., Miao, C., Yu, X., Degan, C., Garcia-Pérez, M., Chen, S., 2015. Two-step
756 microalgal biodiesel production using acidic catalyst generated from pyrolysis-derived bio-
757 char. *Energy Convers. Manage.* 105, 1389-1396.
75817. Dora, S., Bhaskar, T., Singh, R., Naik, D. V., Adhikari, D. K., 2012. Effective catalytic
759 conversion of cellulose into high yields of methyl glucosides over sulfonated carbon based
760 catalyst. *Bioresour. Technol.* 120, 318-321.
76118. Dufour, A., Celzard, A., Fierro, V., Martin, E., Broust, F., Zoulalian, A., 2008. Catalytic
762 decomposition of methane over a wood char concurrently activated by a pyrolysis gas. *Appl.*
763 *Catal. A* 346, 164-173.
76419. El-Rub, Z. A., Bramer, E. A., Brem, G., 2008. Experimental comparison of biomass chars
765 with other catalysts for tar reduction. *Fuel* 87, 2243-2252.
76620. Enslow, K.R., Bell, A.T., 2015. SnCl₄-catalyzed isomerization/dehydration of xylose and
767 glucose to furanics in water. *Catal. Sci. Technol.* 5, 2839-2847.
76821. Fan, Y., Liu, P. F., Yang, Z. J., Jiang, T. W., Yao, K. L., Han, R., Xiong, Y. Y., 2015. Bi-
769 functional porous carbon spheres derived from pectin as electrode material for
770 supercapacitors and support material for Pt nanowires towards electrocatalytic methanol and
771 ethanol oxidation. *Electrochim. Acta* 163, 140-148.
77222. Gallo, J. M. R., Alamillo, R., Dumesic, J. A., 2016. Acid-functionalized mesoporous carbons
773 for the continuous production of 5-hydroxymethylfurfural. *J. Mol. Catal. A: Chem.* 422, 13-
774 17.
77523. Guilminot, E., Gavillon, R., Chatenet, M., Berthon-Fabry, S., Rigacci, A., Budtova, T., 2008.
776 New nanostructured carbons based on porous cellulose: elaboration, pyrolysis and use as
777 platinum nanoparticles substrate for oxygen reduction electrocatalysis. *J. Power Sources* 185,
778 717-726.
77924. Gupta, P., Paul, S., 2011. Amorphous carbon-silica composites bearing sulfonic acid as solid
780 acid catalysts for the chemoselective protection of aldehydes as 1, 1-diacetates and for N-, O-
781 and S-acylations. *Green Chem.* 13, 2365-2372.
78225. Hussain, M., Farooq, M., Nawaz, A., Al-Sadi, A.M., Solaiman, Z.M., Alghamdi, S.S.,
783 Ammara, U., Ok, Y.S., Siddique, K.H., 2017. Biochar for crop production: potential benefits
784 and risks. *J. Soils Sediments* 17, 685-716.
78526. Inyang, M. I., Gao, B., Yao, Y., Xue, Y., Zimmerman, A., Mosa, A., Cao, X., 2016. A review
786 of biochar as a low-cost adsorbent for aqueous heavy metal removal. *Crit. Rev. Env. Sci.*
787 *Tec.* 46, 406-433.
78827. Iwazaki, T., Yang, H., Obinata, R., Sugimoto, W., Takasu, Y., 2010. Oxygen-reduction
789 activity of silk-derived carbons. *J. Power Sources* 195, 5840-5847.
79028. Jin, H., Capareda, S., Chang, Z., Gao, J., Xu, Y., Zhang, J., 2014. Biochar pyrolytically
791 produced from municipal solid wastes for aqueous As (V) removal: Adsorption property and
792 its improvement with KOH activation. *Bioresour. Technol.* 169, 622-629.
79329. Johnson, L., Thielemans, W., Walsh, D. A., 2011. Synthesis of carbon-supported Pt

- 794 nanoparticle electrocatalysts using nanocrystalline cellulose as reducing agent. *Green*
795 *Chem.* 13, 1686-1693.
79630. Kang, S., Ye, J., Zhang, Y., Chang, J., 2013. Preparation of biomass hydrochar derived
797 sulfonated catalysts and their catalytic effects for 5-hydroxymethylfurfural production. *RSC*
798 *Adv.* 3, 7360-7366.
79931. Kastner, J. R., Mani, S., Juneja, A., 2015. Catalytic decomposition of tar using iron supported
800 biochar. *Fuel Process. Technol.* 130, 31-37.
80132. Kastner, J. R., Miller, J., Geller, D. P., Locklin, J., Keith, L. H., Johnson, T., 2012. Catalytic
802 esterification of fatty acids using solid acid catalysts generated from biochar and activated
803 carbon. *Catal. Today* 190, 122-132.
80433. Kastner, J. R., Miller, J., Kolar, P., Das, K. C., 2009. Catalytic ozonation of ammonia using
805 biomass char and wood fly ash. *Chemosphere* 75, 739-744.
80634. Keiluweit, M., Nico, P. S., Johnson, M. G., Kleber, M., 2010. Dynamic molecular structure
807 of plant biomass-derived black carbon (biochar). *Environ. Sci. Technol.* 44, 1247-1253.
80835. Kim, J. R., Kan, E., 2016. Heterogeneous photocatalytic degradation of sulfamethoxazole in
809 water using a biochar-supported TiO₂ photocatalyst. *J. Environ. Manage.* 180, 94-101.
81036. Klinghoffer, N. B., Castaldi, M. J., Nzihou, A., 2015. Influence of char composition and
811 inorganics on catalytic activity of char from biomass gasification. *Fuel* 157, 37-47.
81237. Kobayashi, H., Komanoya, T., Hara, K., Fukuoka, A., 2010. Water-tolerant mesoporous-
813 carbon-supported ruthenium catalysts for the hydrolysis of cellulose to
814 glucose. *ChemSusChem* 3, 440-443.
81538. Komanoya, T., Kobayashi, H., Hara, K., Chun, W.J., Fukuoka, A., 2011. Catalysis and
816 characterization of carbon-supported ruthenium for cellulose hydrolysis. *Appl. Catal. A* 407,
817 188-194.
81839. Kostić, M. D., Bazargan, A., Stamenković, O. S., Veljković, V. B., McKay, G., 2016.
819 Optimization and kinetics of sunflower oil methanolysis catalyzed by calcium oxide-based
820 catalyst derived from palm kernel shell biochar. *Fuel* 163, 304-313.
82140. Kreissl, H.T., Nakagawa, K., Peng, Y.K., Koito, Y., Zheng, J., Tsang, S.C.E., 2016. Niobium
822 oxides: correlation of acidity with structure and catalytic performance in sucrose conversion
823 to 5-hydroxymethylfurfural. *J. Catal.* 338, 329-339.
82441. Lee, J., Kim, K. H., Kwon, E. E., 2017a. Biochar as a catalyst. *Renewable Sustainable*
825 *Energy Rev.* 77, 70-79.
82642. Lee, J., Jung, J. M., Oh, J. I., Ok, Y. S., Lee, S. R., Kwon, E. E., 2017b. Evaluating the
827 effectiveness of various biochars as porous media for biodiesel synthesis via pseudo-catalytic
828 transesterification. *Bioresour. Technol.* 231, 59-64.
82943. Lehmann, J., Kuzyakov, Y., Pan, G., Ok, Y.S., 2015. Biochars and the plant-soil interface.
830 *Plant Soil* 395, 1-5.
83144. Li, M., Zheng, Y., Chen, Y., Zhu, X., 2014. Biodiesel production from waste cooking oil
832 using a heterogeneous catalyst from pyrolyzed rice husk. *Bioresour. Technol.* 154, 345-348.
83345. Li, S., Gu, Z., Bjornson, B. E., Muthukumarappan, A., 2013. Biochar based solid acid
834 catalyst hydrolyze biomass. *J. Environ. Chem. Eng.* 1, 1174-1181.
83546. Li, X., Peng, K., Liu, X., Xia, Q., Wang, Y., 2016. Comprehensive understanding the role of
836 Brønsted and Lewis acid sites in glucose conversion to 5-hydroxymethylfurfural.
837 *ChemCatChem.* <http://dx.doi.org/10.1002/cctc.201601203>.
83847. Li, Y., Zhang, S., Yu, Q., Yin, W., 2007. The effects of activated carbon supports on the
839 structure and properties of TiO₂ nanoparticles prepared by a sol-gel method. *Appl. Surf.*
840 *Sci.* 253, 9254-9258.
84148. Libra, J. A., Ro, K. S., Kammann, C., Funke, A., Berge, N. D., Neubauer, Y., Emmerich, K.
842 H., 2011. Hydrothermal carbonization of biomass residuals: A comparative review of the
843 chemistry, processes and applications of wet and dry pyrolysis. *Biofuels* 2, 71-106.
84449. Lin, Y., Munroe, P., Joseph, S., Henderson, R., Ziolkowski, A., 2012. Water extractable

- 845 organic carbon in untreated and chemical treated biochars. *Chemosphere* 87, 151-157.
84650. Liu, Q. Y., Yang, F., Liu, Z. H., Li, G., 2015a. Preparation of SnO₂-Co₃O₄/C biochar catalyst
847 as a Lewis acid for corncob hydrolysis into furfural in water medium. *J. Ind. Eng. Chem.* 26,
848 46-54.
84951. Liu, W. J., Jiang, H., Yu, H. Q., 2015b. Development of biochar-based functional materials:
850 Toward a sustainable platform carbon material. *Chem. Rev.* 115, 12251-12285.
85152. Lobos, M. L. N., Sieben, J. M., Comignani, V., Duarte, M., Volpe, M. A., Moyano, E. L.,
852 2016. Biochar from pyrolysis of cellulose: An alternative catalyst support for the electro-
853 oxidation of methanol. *Int. J. Hyd. Energy.* 41, 10695-10706.
85453. Ma, M., Dai, Y., Zou, J. L., Wang, L., Pan, K., Fu, H. G., 2014. Synthesis of iron oxide/partly
855 graphitized carbon composites as a high-efficiency and low-cost cathode catalyst for
856 microbial fuel cells. *ACS Appl. Mater. Interfaces* 6, 13438-13447.
85754. Madhu, D., Chavan, S. B., Singh, V., Singh, B., Sharma, Y. C., 2016. An economically viable
858 synthesis of biodiesel from a crude *Milletia pinnata* oil of Jharkhand, India as feedstock and
859 crab shell derived catalyst. *Bioresour. Technol.* 214, 210-217.
86055. McBeath, A. V., Wurster, C. M., Bird, M. I., 2015. Influence of feedstock properties and
861 pyrolysis conditions on biochar carbon stability as determined by hydrogen
862 pyrolysis. *Biomass Bioenergy* 73, 155-173.
86356. Min, Z., Zhang, S., Yimsiri, P., Wang, Y., Asadullah, M., Li, C. Z., 2013. Catalytic reforming
864 of tar during gasification. Part IV. Changes in the structure of char in the char-supported iron
865 catalyst during reforming. *Fuel* 106, 858-863.
86657. Mohan, D., Sarswat, A., Ok, Y. S., Pittman, C. U., 2014. Organic and inorganic contaminants
867 removal from water with biochar, a renewable, low cost and sustainable adsorbent—a critical
868 review. *Bioresour. Technol.* 160, 191-202.
86958. Morone, A., Apte, M., Pandey, R. A., 2015. Levulinic acid production from renewable waste
870 resources: Bottlenecks, potential remedies, advancements and applications. *Renewable*
871 *Sustainable Energy Rev.* 51, 548-565.
87259. Muradov, N., Fidalgo, B., Gujar, A. C., Garceau, N., Ali, T., 2012. Production and
873 characterization of *Lemna minor* bio-char and its catalytic application for biogas
874 reforming. *Biomass Bioenergy* 42, 123-131.
87560. Norouzi, O., Jafarian, S., Safari, F., Tavasoli, A., Nejati, B., 2016. Promotion of hydrogen-
876 rich gas and phenolic-rich bio-oil production from green macroalgae *Cladophora glomerata*
877 via pyrolysis over its bio-char. *Bioresour. Technol.* 219, 643-651.
87861. Ok, Y.S., Chang, S.X., Gao, B., Chung, H.J., 2015. SMART biochar technology—a shifting
879 paradigm towards advanced materials and healthcare research. *Environ. Technol. Innovation*
880 4, 206-209.
88162. Ormsby, R., Kastner, J.R., Miller, J. 2012, Hemicellulose hydrolysis using solid acid catalysts
882 generated from biochar. *Catalysis Today* 190, 89-97.
88363. Osatiashtiani, A., Lee, A.F., Brown, D.R., Melero, J.A., Morales, G., Wilson, K., 2014.
884 Bifunctional SO₄/ZrO₂ catalysts for 5-hydroxymethylfurfural (5-HMF) production from
885 glucose. *Catal. Sci. Technol.* 4, 333-342.
88664. Qian, K., Kumar, A., Zhang, H., Bellmer, D., Huhnke, R., 2015. Recent advances in
887 utilization of biochar. *Renewable Sustainable Energy Rev.* 42, 1055-1064.
88865. Rajapaksha, A.U., Chen, S.S., Tsang, D.C.W., Zhang, M., Vithanage, M., Mandal, S., Ok, Y.
889 S., 2016a. Engineered/designer biochar for contaminant removal/immobilization from soil
890 and water: Potential and implication of biochar modification. *Chemosphere* 148, 276-291.
89166. Rajapaksha, A.U., Vithanage, M., Lee, S.S., Seo, D.C., **Tsang, D.C.W.**, Ok, Y.S., 2016b.
892 Steam activation of biochars facilitates kinetics and pH-resilience of sulfamethazine sorption.
893 *J. Soils Sediments*, 16, 889-895.
89467. Rizwan, M., Ali, S., Qayyum, M. F., Ibrahim, M., Zia-ur-Rehman, M., Abbas, T., Ok, Y. S.,
895 2016. Mechanisms of biochar-mediated alleviation of toxicity of trace elements in plants: a

- 896 critical review. *Environ. Sci. Pollut. Res.* 23, 2230-2248.
89768. Shen, B., Chen, J., Yue, S., Li, G., 2015a. A comparative study of modified cotton biochar
898 and activated carbon based catalysts in low temperature SCR. *Fuel* 156, 47-53.
89969. Shen, Y., Chen, M., Sun, T., Jia, J., 2015b. Catalytic reforming of pyrolysis tar over metallic
900 nickel nanoparticles embedded in pyrochar. *Fuel* 159, 570-579.
90170. Shen, Y., Yoshikawa, K., 2014. Tar conversion and vapor upgrading via in situ catalysis using
902 silica-based nickel nanoparticles embedded in rice husk char for biomass
903 pyrolysis/gasification. *Ind. Eng. Chem. Res.* 53, 10929-10942.
90471. Smith, S.M., Oopathum, C., Weeramongkhonlert, V., Smith, C.B., Chaveanghong, S.,
905 Ketwong, P., Boonyuen, S., 2013. Transesterification of soybean oil using bovine bone waste
906 as new catalyst. *Bioresour. Technol.* 143, 686-690.
90772. Tan, X., Liu, Y., Zeng, G., Wang, X., Hu, X., Gu, Y., Yang, Z., 2015. Application of biochar
908 for the removal of pollutants from aqueous solutions. *Chemosphere* 125, 70-85.
90973. Tang, J., Zhu, W., Kookana, R., Katayama, A., 2013. Characteristics of biochar and its
910 application in remediation of contaminated soil. *J. Biosci. Bioeng.* 116, 653-659.
91174. Tao, F., Song, H., Chou, L., 2011. Catalytic conversion of cellulose to chemicals in ionic
912 liquid. *Carbohydr. Res.* 346, 58-63.
91375. Tsilomelekis, G., Orella, M.J., Lin, Z., Cheng, Z., Zheng, W., Nikolakis, V., Vlachos, D.G.,
914 2016. Molecular structure, morphology and growth mechanisms and rates of 5-
915 hydroxymethyl furfural (HMF) derived humins. *Green Chem.* 18, 1983-1993.
91676. Umeyama, T., Imahori, H., 2013. Photofunctional hybrid nanocarbon materials. *J. Phys.*
917 *Chem.* 117, 3195-3209.
91877. Wang, J., Zhu, L., Wang, Y., Cui, H., Zhang, Y., Zhang, Y., 2016. Fructose dehydration to 5-
919 HMF over three sulfonated carbons: effect of different pore structures. *J. Chem. Technol.*
920 *Biotechnol.* 92, 1454-1463.
92178. Wang, S., Wang, H., Yin, Q., Zhu, L., Yin, S., 2014. Methanation of bio-syngas over a
922 biochar supported catalyst. *New J. Chem.* 38, 4471-4477.
92379. Wei, W., Wu, S., 2017. Experimental and kinetic study of glucose conversion to levulinic
924 acid catalyzed by synergy of Lewis and Brønsted acids. *Chem. Eng. J.* 307, 389-398.
92580. Yan, Q., Wan, C., Liu, J., Gao, J., Yu, F., Zhang, J., Cai, Z., 2013. Iron nanoparticles in situ
926 encapsulated in biochar-based carbon as an effective catalyst for the conversion of biomass-
927 derived syngas to liquid hydrocarbons. *Green Chem.* 15, 1631-1640.
92881. Yang, H., Yan, R., Chen, H., Lee, D. H., Zheng, C., 2007. Characteristics of hemicellulose,
929 cellulose and lignin pyrolysis. *Fuel* 86, 1781-1788.
93082. Yao, D., Hu, Q., Wang, D., Yang, H., Wu, C., Wang, X., Chen, H., 2016. Hydrogen
931 production from biomass gasification using biochar as a catalyst/support. *Bioresour.*
932 *Technol.* 216, 159-164.
93383. Yu, I.K.M., Tsang, D.C.W., 2017. Conversion of biomass and carbohydrates to
934 hydroxymethylfurfural: a review of catalytic systems and underlying mechanisms. *Bioresour.*
935 *Technol.* 238, 716-732.
93684. Yu, I.K.M., Tsang, D.C.W., Yip, A.C.K., Chen, S.S., Ok, Y.S., Poon, C.S., 2016. Valorization
937 of food waste into hydroxymethylfurfural: Dual role of metal ions in successive conversion
938 steps. *Bioresour. Technol.* 219, 338-347.
93985. Yu, I.K.M., Tsang, D.C.W., Yip, A.C.K., Chen, S.S., Ok, Y.S., Poon, C.S., 2017a.
940 Valorization of starchy, cellulosic, and sugary food waste into hydroxymethylfurfural by one-
941 pot catalysis. *Chemosphere* 184, 1099-1107.
94286. Yu, I.K.M., Tsang, D.C.W., Yip, A.C.K., Chen, S.S., Wang, L., Ok, Y.S., Poon, C.S., 2017b.
943 Catalytic valorization of starch-rich food waste into hydroxymethylfurfural (HMF):
944 controlling relative kinetics for high productivity. *Bioresour. Technol.* 237, 222-230.
94587. Yuan, Y., Yuan, T., Wang, D., Tang, J., Zhou, S., 2013. Sewage sludge biochar as an efficient
946 catalyst for oxygen reduction reaction in an microbial fuel cell. *Bioresour. Technol.* 144, 115-

- 947 120.
94888. Zhang, C., Cheng, Z., Fu, Z., Liu, Y., Yi, X., Zheng, A., Kirk, S.R., Yin, D., 2017. Effective
949 transformation of cellulose to 5-hydroxymethylfurfural catalyzed by fluorine anion-
950 containing ionic liquid modified biochar sulfonic acids in water. *Cellulose* 24, 95-106.
95189. Zhang, C., Liang, X., Liu, S., 2011a. Hydrogen production by catalytic dehydrogenation of
952 methylcyclohexane over Pt catalysts supported on pyrolytic waste tire char. *Int. J. Hyd.*
953 *Energy*. 36, 8902-8907.
95490. Zhang, S., Jin, F., Hu, J., Huo, Z., 2011b. Improvement of lactic acid production from
955 cellulose with the addition of Zn/Ni/C under alkaline hydrothermal conditions. *Bioresour.*
956 *Technol.* 102, 1998-2003.
95791. Zhang, X., Wilson, K., Lee, A. F., 2016. Heterogeneously catalyzed hydrothermal processing
958 of C₅-C₆ sugars. *Chem. Rev.* 116, 12328-12368.
95992. Zhou, C. H., Xia, X., Lin, C. X., Tong, D. S., Beltramini, J., 2011. Catalytic conversion of
960 lignocellulosic biomass to fine chemicals and fuels. *Chem. Soc. Rev.* 40, 5588-5617.
96193. Zhou, T., Wang, H., Ji, S., Feng, H., Wang, R., 2014. Synthesis of mesoporous carbon from
962 okara and application as electrocatalyst support. *Fuel Cells* 14, 296-302.
- 963